Dynamics of heterogeneous wetting in periodic hybrid nanopores

Cyril Picard, Valentin Gérard, Loïc Michel, X. Cattoen, Elisabeth Charlaix

Dynamics of heterogeneous wetting in periodic hybrid nanopores

C. Picard,[1] V. Gerard,[1] L. Michel,[1] X. Cattoen,[2] and E. Charlaix [1a)]
[1)] *Univ. Grenoble Alpes, CNRS, LIPhy, 38000 Grenoble, France*
[2)] *Univ. Grenoble Alpes, CNRS, Grenoble INP, Institut Néel, 38000 Grenoble, France*

(Dated: 16 January 2021)

We present experimental and theoretical results concerning the forced filling and spontaneous drying of hydrophobic cylindrical mesopores in dynamical regime. Pores are structured with organic/inorganic moieties responsible for a periodicity of the surface energy along their axis. We find that the forced intrusion of water in these hydrophobic pores presents a slow dynamics: the intrusion pressure decreases as the logarithm of the intrusion time. We find that this slow dynamics is well described quantitatively by a classical model of activated wetting at the nanoscale, giving access to the structural length scales and surface energies of the mesoporous material.

I. INTRODUCTION

The wetting of micro- and mesoporous hydrophobic materials has long been studied in relation with the storage of surface energy[1]. The pionnering work of Eroshenko[2,3], studying the intrusion and extrusion of water in hydrophobic nanopores to store and retrieve mechanical energy, started a very active field of research on the wetting and drying of lyophobic nanoporous materials, with potential applications for the design of new energy storage devices[4–9].

Among the many micro- and mesoporous materials which have been studied, micelle-templated silicas (MTS's) revealed themselves as an ideal laboratory for studying wetting at a nanoscale with an ultimately simple and well-controlled geometry. The highly regular cylindrical shape of pores in materials such as MCMs or SBAs[10,11] allowed to challenge in depth the concepts of macroscopic thermodynamics such as casting systems into bulk, surfaces and lines, and to confront the robustness and validity of this picture at the nanoscale**?** . More specifically by varying the pore size of MTS's it was shown that the intrusion pressure follows the Laplace law of capillarity down to a pore radius of 1.3 nm, validating the macroscopic concept of converting bulk energy into purely interfacial energy[12,13]. Similarly, the thermically activated extrusion process observed in dynamic studies, was confronted to a first-order phase transition triggered by the nucleation of a nanobubble[12,14]: macroscopic capillarity provided an excellent quantitative prediction of the nucleus volume for a variety of MTS's, allowing a first experimental estimation of the sign and maximum amplitude of the water/solid/vapor line tension[15–18].

However as noted by Fraux et al in their review[1], hydrophobic surfaces in real life are heterogeneous, and the question of the phase-stability and wetting behaviour of water confined between heterogeneous hydrophobic surfaces is common to a variery of materials, from biological cavities and porous polymers to inorganic and other open framework porous materials. In this article we address this question by using Periodic Mesoporous Organosilicas (PMOs)[19], which are silica/organic materials combining the cylindrical pore-shape of MCMs and SBAs with a periodic nano-scale alternance of the internal surface chemistry. These materials thus provide an ideally simple periodic heterogeneity. The first studies of intrusion-extrusion of water and lyophobic solutions in hydrophobized PMOS have shown their high interest for energy storage applications[20]. Here we specifically address the dynamics of the intrusion-extrusion processes, which is of importance to qualify the power density in energetic applications. We find that unlike MCMs and SBAs, both intrusion and extrusion pressure of water in PMOs exhibit a logarithmic kinetics. In MCMs and SBAs this logarithmic kinetics was observed only for extrusion[15]. We show that in PMOS, the logarithmic kinetics of both intrusion and extrusion process can be quantitatively described by a classical model of heterogeneous wetting[21–24] based on thermically activated jumps of the liquid meniscus over nanoscale anchoring defects. The excellent quantitative agreement with the periodic feature of PMOS allows us to conclude that dynamic intrusion/extrusion experiments in lyophobic nanomaterials can provide a quantitative characterization of the internal heterogeneity of these nanomaterials. We discuss the relative importance of contact line pinning over nanoscale defects, and nucleation of nanobubbles/drops, for triggering the filling or drying of cylindrical mesopores.

II. EXPERIMENTAL SECTION

A. Periodic mesoporous organosilicas as model nanopores with ordered defects

Periodic mesoporous organosilicas (PMOs) are ordered micelle-templated matrices. Unlike micelle-templated pure silicic structure such as MCM-41, PMOs are made of several chemical-moieties organized in crystal-like pore walls which feature periodic physico-chemical properties.[25,26]. The PMO chosen for this study consists of independent quasi-cylindrical nanopores structured as a succession of silica/benzene annuli and first synthesized be Inagaki *et al* in 1999[27]. Pores organize as a two-dimensional hexagonal lattice (see Fig. 1). The material is synthesized following Inagaki *et al* (see appendix A). The nitrogen adsorption characterization leads to a specific mesopore volume of $V_n = 0.57$ cm^3/g and a specific area of 760 m2/g which are respectively 16% and 8% smaller than

[a)]Electronic mail: elisabeth.charlaix@univ-grenoble-alpes.fr

the one given by Inagaki potentially because of a larger number of defects in our material. From a modeling of the nitrogen adsorption isotherm[28–30] we find a pore radius of 1.95 nm (see appendix B), while Inagaki et al indicate a radius of 1.9 nm for their material. From X-ray diffraction, the inter-reticular distance is 4.6 nm for which agrees with the value of 4.55 nm given by Inagaki *et al*. Based on this good agreement, we expect that the periodicity along the pore axis of our material presents the same periodicity of 0.77 nm as given by Inagaki et al[27].

This native material although more hydrophobic than a purely silicic matrix requires a grafting of silica annuli to reach a hydrophobicity strong enough to be compatible with intrusion/extrusion experiments. For this purpose we follow a protocol optimized for the hydrophobization of MCM-41 based on covalent grafting of *n*-octyl-dimethylchlorosilane onto surface silanol groups (see ppendix A)[12]. Fitting of the same model as the one used for the native material leads to an average pore radius $R_p = 1.5$ nm for the grafted material (see appendix B). For a plain silica MCM-41 approximately the same size of our PMO, grafted with the very same protocol on its whole surface, Guillemot et al[15] obtained a grafted pore radius of 1.34 nm for a pristine pore radius of 2.07 nm. The difference between these two radii is almost twice the difference between R_w and R_p measured in our PMO. The reason is attributed to the fact that grafting concerns inorganic annuli only, which correspond approximately to half the total surface of the PMO, based on the simple geometric view given by Inagaki *et al*[27]. In other words we expect that the grafted annuli in our PMO present a radius close to the one measured in the fully grafted MCM-41 typically $R_s = 1.3$ nm (corresponding to regions of strong hydrophobicity) while the non grafted organic annuli (corresponding to regions of week hydrophobicity) would keep the radius $R_w = 1.95$ nm of the native material. The radius R_p comprised between R_s and R_w results from the effective portion of the surface which is silanized.

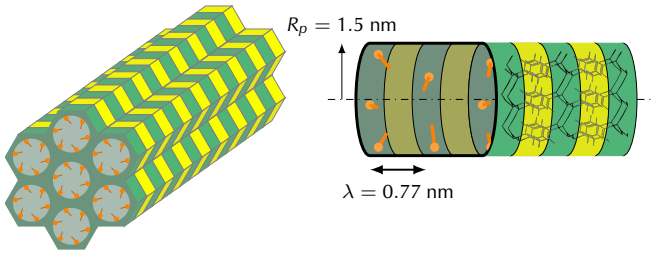

FIG. 1. Schematics of the 2D hexagonal structure of PMO with a axial periodicity of silica (green) and benzene (yellow) parts. Right : zoom on a single nanopore, the inside of which is silanized (grafting agent symbolized in orange) on silica annulus only.

The thermo-gravimetric analysis of the material, leads to an average grafting agent density on the wall of 0.7 nm^{-2} based on the total native material surface. Considering that silica annuli stand for half the surface of the pore this leads to a grafting density of 1.4 nm^{-2}. This value is close to the value of 1.3 nm^{-2} given by Lefevre *et al*[13] obtained when grafting pure silicic MCM-41. This suggest that approximately half of the PMO surface is indeed grafted in agreement with the expected structure of the pores.

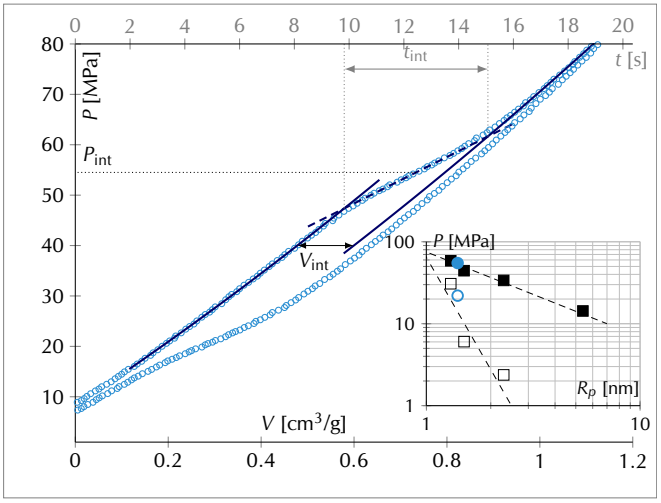

FIG. 2. Raw intrusion/extrusion isotherm of water in silanized PMO for 1 g of porous material. Markers are measured pressure according to volume reduction (bottom axis) or time for the compression stage (top axis). Full lines are fitting of compression before and after intrusion. The dashed line is a linear fitting of the intrusion plateau. Inset : comparison of the intrusion (full symbols) and extrusion (open symbols) pressures for water/MCM-41 (black symbols) from Lefevre et al[12] and for water/PMO (blue symbols) used in this work. Dahsed lines are guides for the eye.

B. Water intrusion-extrusion study

Water intrusion/extrusion experiments where performed on a home-made dynamical intrusiometer that will be fully described elsewhere. This thermally regulated apparatus, driven by a traction machine (MTS 810) is able to cover four decades of intrusion/extrusion time-scale down to 10 ms with an almost elastic behavior in absence of sample that is perfectly preserved on the full range of time scale[33]. The sample made of a suspension of 490 mg of PMO in water is placed into a dedicated deformable container immersed in glycerol as a pressure transmitting fluid within the measurement chamber of the apparatus. A raw intrusion/extrusion cycle obtained with this sample is shown in Fig. 2. This cycle demonstrates for the first time that a silanised PMO can be used as a high pressure fully reversible Lyophobic Heterogeneous System. This result extends the behavior previously observed with another PMO type which led to irreversible behavior[31]. Our grafted sample, which demonstrates a good stability, has been used for more than 4 h of cumulative intruded time. As detailed in section V, a slow decrease of pressures is nevertheless observed according to the time the material spends in its filled state, presumably related to the hydrolysis of silane. Three main indicators are extracted from raw intrusion/extrusion data. The first quantity is the average intrusion pressure P_{int}, respectively the extrusion pressure P_{ext}. The second quantity is the intruded volume V obtained from a subtraction to the

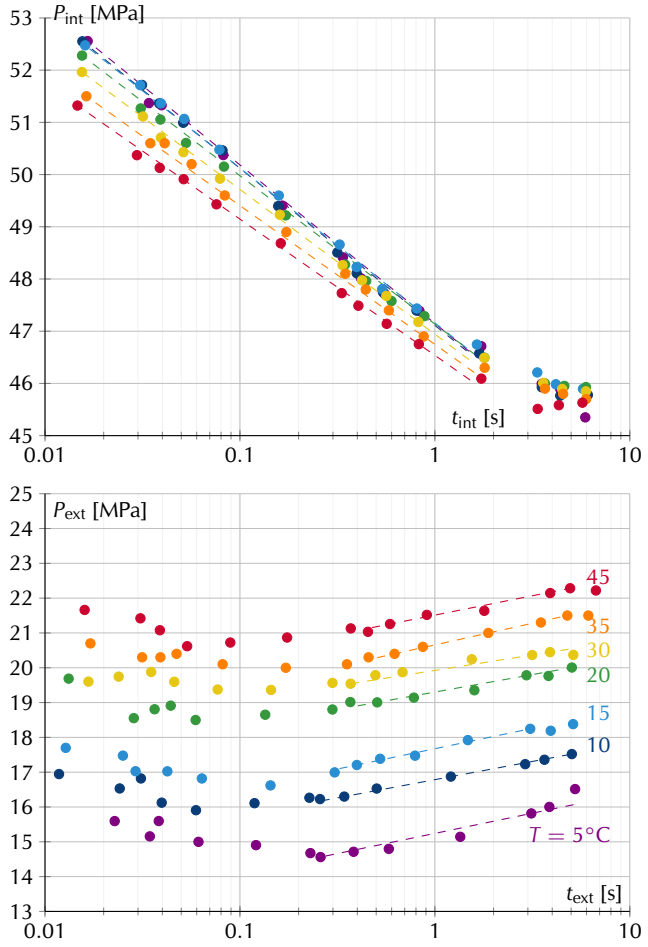

FIG. 3. Intrusion pressure P_{int} (upper graph) and extrusion pressure P_{ext} (lower graph) of water into PMO as a function respectively of the intrusion time t_{int} and extrusion time t_{ext} for temperature from 5°C to 45°C as indicated on the lower graph. Dots are experimental values, dashed line are linear fits.

raw data of the elastic deformation of the system. The third quantity is the intrusion duration $t_{\rm int}$, respectively $t_{\rm ext}$, required to cover the intrusion/extrusion plateaus.

As shown in the inset of Fig. 2, the values of $P_{\rm int}$ and $P_{\rm ext}$, measured at low speed with the PMO, are in good agreement with the trend that can be interpolated from the values previously obtained with MCM-41[12].

C. Slow dynamics of forced wetting in hydrophobized PMOS

When exploring the dynamical regime, one observes both for intrusion and extrusion pressures a slow dependance on respective intrusion and extrusion time. The intrusion pressure follows an almost linear decrease with the logarithm of intrusion time on two decades of times, while the extrusion pressure follows an almost linear increase with the logarithm of extrusion time on approximately one decade of time (see dashed lines in Fig. 3). However, beyond this common logarithmic trend, several differences should be noted. First, the logarithmic trend is observed for the intrusion at short time up 2 s approximately while for the extrusion this behavior is valid only beyond 100 ms. At long time for the intrusion, the decrease of P_{int} seems to be slower than the logarithmic behavior at short time. At short time for the extrusion, one observe a sudden stabilization of P_{ext} to not say a non intuitive increase of P_{ext} when t_{ext} decreases. Second, the slope of the logarithmic regime is much more pronounced for the intrusion than for the extrusion. This fact contrasts with results obtained with MCM-41 with similar radius for which the opposite trend is observed, that is a stronger variation with time of P_{ext} than P_{int}. Third, P_{ext} shows a dependance of its offset on temperature which is much less pronounced for P_{int}. In addition one notice a slight decrease of the logarithmic slope with temperature for the intrusion, while the slope remains almost unchanged for the extrusion.

III. THERMICALLY ACTIVATED WETTING IN HETEROGENOUS NANOPORES

We consider the motion of a liquid meniscus in a cylinder featuring a periodic step-wise alternance of radius and wall chemistry. The pore wall is characterized by its local wettability, i.e. the local solid-vapor and solid-liquid surface tension with associated equilibrium Young's contact angle:

$$\gamma_{SV,w} - \gamma_{SL,w} = \gamma_{LV}\cos\theta_w \quad (1)$$

$$\gamma_{SV,s} - \gamma_{SL,s} = \gamma_{LV}\cos\theta_s \quad (2)$$

$$\cos\theta_s < \cos\theta_w \leq 0 \quad (3)$$

The index w (resp. s) refers to the pore portion which is weakly (resp. strongly) hydrophobic. The length, radius and volume of each portion are respectively $V_{s,w} = \pi R_{s,w}^2 l_{s,w}$. The wave length of the periodic pattern $\lambda = l_s + l_w$.

The pore is connected to a liquid reservoir at pressure P. The free energy of the system when the liquid interface is located at a distance x from the pore entrance is

$$\mathscr{F}(x) = -P\int_0^x \pi R(x')^2 dx' + \int_0^x 2\pi R(x')\mathscr{E}(x')dx' \quad (4)$$

$$\mathscr{E}(x') = (\gamma_{SL} - \gamma_{SV})(x') \quad (5)$$

with $\mathscr{E}(x)$ and $R(x)$ the local surface energy and pore radius at abcissa x.

The equilibrium pressures $P_{int,o}$ and $P_{ext,o}$ on each portion are obtained from the local condition $(d\mathscr{F}/dx)_{s,w} = 0$

$$P_{int,o} = -\frac{2\gamma_{LV}\cos\theta_s}{R_s} \quad P_{ext,o} = -\frac{2\gamma_{LV}\cos\theta_w}{R_w} \quad (6)$$

The global equilibrium pressure P_{eq} for which $\mathscr{F}(x)$ is periodic is defined by $l_s(d\mathscr{F}/dx)_s + l_w(d\mathscr{F}/dx)_w = 0$

$$P_{eq} = \frac{V_s P_{int,o} + V_w P_{ext,o}}{V_s + V_w} = -\frac{2\gamma_{LV}\cos\theta_{CB}}{R_p} \quad (7)$$

$$R_p = \frac{2V_{tot}}{A_{tot}} = \frac{V_s + V_w}{\pi R_s l_s + \pi R_w l_w} \quad (8)$$

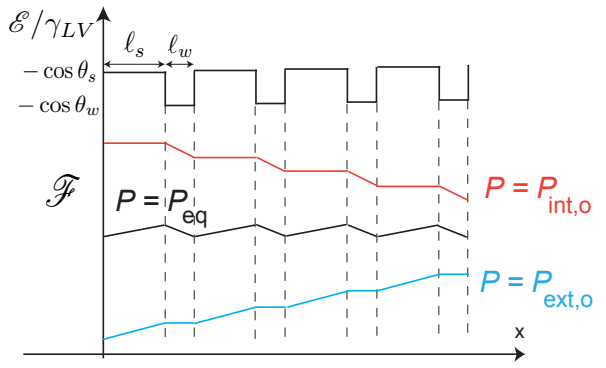

FIG. 4. Plot of eqs (4) and (5): local surface energy $\mathscr{E}/\gamma_{LV}$, and free energy $\mathscr{F}(x)$ of the system at position x of the meniscus.

R_p is the average pore size and θ_{CB} is the Cassie-Baxter contact angle.

When the reservoir pressure P is equal to $P_{int,o}$ the liquid can penetrate in the pore without having to overcome any energy barrier. Symmetrically if $P = P_{ext,o}$, the liquid meniscus can freely receed up to the pore entrance. But if $P_{int,o} < P < P_{ext,o}$ the meniscus spends most of its time pinned in the local minima of the free energy, which are at the junction of a weakly hydrophobic portion on the x^- side and a strongly hydrophobic portion on the x^+ side. The energy barrier ΔE^+ (resp ΔE^-) for reaching the next minimum on the x^+ side (resp x^- side) are

$$\Delta E^+ = l_s \left(\frac{\partial \mathscr{F}}{\partial x}\right)_s = V_s(P_{int,o} - P) > 0 \qquad (9)$$

$$\Delta E^- = -l_w \left(\frac{\partial \mathscr{F}}{\partial x}\right)_w = V_w(P - P_{ext,o}) > 0 \qquad (10)$$

It is of interest to express these barriers as a function of P_{eq}

$$\Delta E^+ = -V_s(P - P_{eq}) + \mathscr{E}_{def}$$
$$\Delta E^- = V_w(P - P_{eq}) + \mathscr{E}_{def}$$

$$\mathscr{E}_{def} = V_s(P_{int,o} - P_{eq}) = V_w(P_{eq} - P_{ext,o}) \qquad (11)$$

where $\mathscr{E}_{def}$ represents a defect energy. In a thermically activated process the number of jumps in the x^+ direction (resp. the x^- direction) per unit time is $n^\pm = \nu_o \exp(-\Delta E^\pm/k_BT)$ where ν_o is an attempt frequency characterizing the local meniscus dynamics, and the length of each jump is $\pm\lambda$. The average liquid velocity $V = \lambda\nu_o(n^+ - n^-)$ writes as

$$V = \lambda\nu_o e^{-\mathscr{E}_{def}/k_BT}\left(e^{V_s(P-P_{eq})/k_BT} - e^{-V_w(P-P_{eq})/k_BT}\right) \qquad (12)$$

A pressure value $P > P_{eq}$ corresponds to $V > 0$ and a wetting process, whereas a value $P < P_{eq}$ corresponds to a drying process. It is of interest to introduce the short cut-off time t_o and the large cross-over time τ:

$$t_o = \frac{L_P}{\lambda\nu_o} \qquad \tau = t_o e^{\mathscr{E}_{def}/k_BT} \qquad (13)$$

where L_P is the pore length. The intrusion and extrusion times are given respectively by:

$$\frac{\tau}{t_{int}} = e^{V_s(P_{int}-P_{eq})/k_BT} - e^{-V_w(P_{int}-P_{eq})/k_BT} \qquad (14)$$

$$\frac{\tau}{t_{ext}} = e^{V_w(P_{eq}-P_{ext})/k_BT} - e^{-V_s(P_{eq}-P_{ext})/k_BT} \qquad (15)$$

If P si significantly larger (resp. lower) than P_{eq} one can neglect the exponential term of negative argument and get a purely logarithmic kinetics:

$$P_{int} = P_{int,o} - \frac{k_BT}{V_s}\ln\frac{t_{int}}{t_o} \quad P \gg P_{eq} \qquad (16)$$

$$P_{ext} = P_{ext,o} + \frac{k_BT}{V_w}\ln\frac{t_{ext}}{t_o} \quad P \ll P_{eq} \qquad (17)$$

The slopes of the logarithmic kinetics are proportionnal to the inverse of the volume of the anchoring defects, in both directions of motion. Small size heterogeneities thus contribute to a large amplitude of the logarithmic kinetics of the intrusion and extrusion pressures.

Eq. (16) and (17) also show that the logarithmic kinetics has a limited range in time, which is the same for intrusion and extrusion. At short time $t < t_o$, too many activated jumps are needed to fill or empty the pores in the required time: the intrusion/extrusion processes can occur only when there is no barrier, respectively at $P_{int,o}$ and $P_{ext,o}$. Thus the cut-off time t_o is the onset of the logarithmic kinetics. At larger times, the logarithmics kinetics saturates to the equilibrium pressure. Eq. (16) and (17) give the cross-over time for this saturation, which is equal to τ, both for the intrusion and extrusion processes.

IV. COMPARISON WITH EXPERIMENTAL RESULTS: INTRUSION.

As the logarithmic decay of the experimental intrusion pressure shows a weakening at times larger than 2s (see Fig.3), we use the full eq. (14) to compare the experimental intrusion pressure to the model of activated wetting. In principle Eq. (14) has 4 adjustable parameters: P_{eq}, V_s, V_w and the cross-over time τ. However we obtain only 3 reliable parameters from the fit of the intrusion pressure. The volume V_w does not influence much the shape of the theoretical curve, and consequently it cannot be determined. More specifically we have tried 3 fitting conditions: V_w left free to vary (but it can then take non-physical values), V_w forced to 0, and $V_w = \pi R_P^2(\lambda - l_s)$ assuming the value $\lambda = 0.77$ nm. The values of the parameters P_{eq}, V_s and τ found with these 3 different conditions change less than 5%. Their value for the range of temperature studied is gathered in table (III) and the result of the fit is plotted in Figure (5).

A. Volume of the strongly hydrophobic regions and Cassie-Baxter contact angle.

The volume V_s of the strongly hydrophobic portion of the pore is found to lie between 2.7 nm^3 and 3.6 nm^3, which cor-

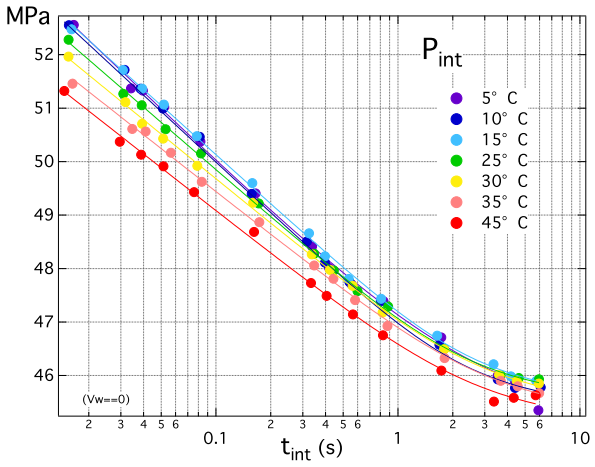

FIG. 5. Fit of the intrusion pressure for various temperatures by eq(14).

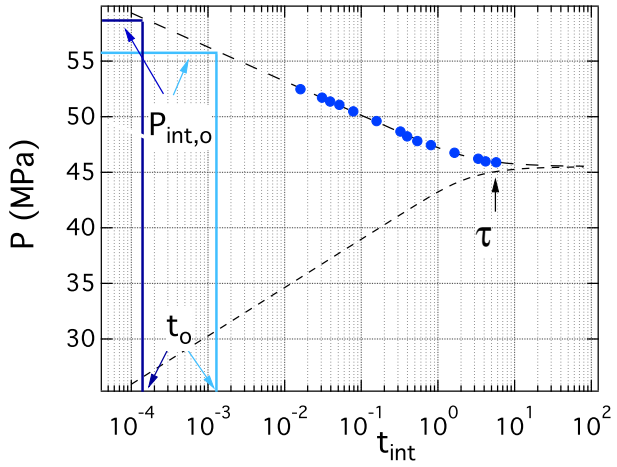

FIG. 6. Dashed line: prediction of eq. (14) for the intrusion pressure at $T = 15°$C. At short time $t < t_o = L_P/\lambda\nu_o$ the intrusion pressure saturates to $P_{int,o}$. Two values of t_o are sketched: $\nu_o = 1$ MHz (light blue) giving $P_{int,o}$=53.8 MPa, and $\nu_o = 10$ MHz (dark blue) giving $P_{int,o}$=56.8 MPa.

responds to a length $l_s = V_s/\pi R_s^2$ between 0.51 nm to 0.69 nm. This value is compatible with the expected PMOs structure, although larger than half the period $\lambda/2 = 0.385$ nm, which is the expected extension of each domains of the hybrid pores. This could be due to the finite size of the C8 silane molecules used for the grafting, which could partially extend onto the organic portion of the pores close to the organic/silica boundary. In this view, the slight increase of l_s with the temperature, of the order of 0.16 nm, could be associated to an increased "thickness" of the grafted-silica/organic boundary under the effect of increased thermal fluctuations.

The equilibrium pressure P_{eq} gives access through Eq. (8) to the Cassie-Baxter contact angle, as well as to the average pore surface energy $(\gamma_{SL} - \gamma_{SV}) = -2\gamma_{LV}\cos\theta_{CB} = P_{eq}R_p/2$. The average pore surface energy $(\gamma_{SL} - \gamma_{SV})$ is essentially independant of the temperature and has a value of 33.8 $\pm$0.2 mN/m. This quasi-absence of temperature variation is attributed to the fact that the solid interface is weakly affected by thermal fluctuations. The Cassie-Baxter contact angle is found to increase from 116.8° to 119.3° in the temperature range 5°C-45°C. This variation of θ_{CB} with the temperature is a pure consequence of the decrease of the water surface tension $\gamma_{LV}(T)$ with temperature, reaching 10% of relative variation in our temperature range.

Finally the properties of the weakly hydrophobic parts of the pore can be evaluated indirectly using the relation $V_w = V_s(R_s^{-1} - R_p^{-1})/(R_p^{-1} - R_w^{-1})$ obtained from eq. (8). For the average value of the intrusion volume $V_s = 3.2$ nm and hydrophobic length $l_s = 0.6$ nm, we find $V_w = 2.13$ nm, $l_w = V_w/\pi R_w^2 = 0.18$ nm, and $l_s + l_w = 0.78$ nm, a value very close to the period $\lambda = 0.77$ nm first determined by Inagaki et al[27].

TABLE I. Raw parameters V_s, P_{eq} and τ obtained from fitting the intrusion pressure with eq. (14). The length of the strongly hydrophobic parts of the pores is $l_s = V_s/\pi R_s^2$ with $R_s = 1.3$ nm, the Cassie-Baxter contact angle θ_{CB} and the average pore surface energy $\gamma_{SL} - \gamma_{SV} = R_P P_{eq}/2$ are obtained from eq. (8) with R_p=1.5 nm.

T °C	V_s nm^3	P_{eq} MPa	τ s	l_s nm	θ_{CB} °	$\gamma_{SL} - \gamma_{SV}$ mN/m
5	2.7	45.17	3	0.51	116.9	33.9
10	2.73	45.1	3.1	0.52	117.1	33.8
15	2.87	45.2	3.3	0.54	117.5	33.9
25	3.08	45.3	2.83	0.58	118.1	34
30	3.35	45.2	3.5	0.63	118.4	33.9
35	3.56	45.0	3.8	0.67	118.7	33.8
45	3.67	44.9	3.1	0.69	119.3	33.7

B. Time extension of the logarithmic kinetics.

Regarding the cross-over time τ, we extract from eq. (11) and (16) the following relation

$$P_{int,o} = P_{eq} + \frac{k_B T}{V_s}\ln\frac{\tau}{t_o} \qquad t_o = \frac{L_p}{\lambda\nu_o} \tag{18}$$

The unknown parameter t_o entering in the logarithmic term has to be estimated. We assume $\lambda = 0.77$ nm, and take $L_P = 1$ μm as the average length of pores in PMOs powder. The estimation of the frequency ν_o is less straightforward. Clearly a jump of the meniscus implies a displacement of the whole liquid column, and cannot be ascribed to a purely molecular mechanism. It is thus more relevant to consider the typical frequency of the liquid meniscus in the nanopore. The frequency response of a meniscus in a cylindrical capillary, studied by Gayvallet et al[32], is flat up to a cut-off frequency $\nu_m = \omega_o^2/2\pi\omega_c$ where $\omega_o^2 = 2\gamma_{LV}\sin\theta(1+\sin\theta)^2/\rho L_P R_P^2$ is the angular frequency of undamped oscillation, and $\omega_c = 8\eta/\rho R_p^2$ is the angular frequency associated to the viscous damping in a cylindrical tube. Above ν_m the motion of the liquid is overdamped. Used in a PMOs nanopore with a contat angle lying between 90° and 120° the cut-off frequency

TABLE II. Range of values of $P_{int,o}$ obtained for ν_o lying between 1-10 MHz. The contact angle θ_s on the most hydrophobic part of the pore, and the solid surface energy of this grafted part $(\gamma_{SL}-\gamma_{SV})_s$, are calculated from $P_{int,o}$ using eq. (18). nm.

T °C	$P_{int,o}$ MPa	θ_s mN/m	$(\gamma_{SL}-\gamma_{SV})_s$
5	56.2-59.5	120 ± 1	43.4 ± 1.2
10	56.3-59.6	120.5 ± 1	43.5 ± 1.2
15	56.2-59.4	120.7 ± 1	43.3 ± 1.2
25	55.6-58.7	121 ± 1	42.9 ± 1.2
30	55.1-58.	121.1 ± 1	42.4 ± 1.2
35	54.7-57.4	121.3 ± 0.9	42 ± 1.2
45	54.3-57.1	121.7 ± 0.9	41.7 ± 1.2

is $\nu_m \sim 1$ MHz. At higher frequencies the liquid column is pinned by viscosity, and fluctuations of the meniscus position can occur only at the expense of local dilatation/compression of the liquid, requiring a higher potential energy.

The trial value $\nu_o = 1$MHz gives $t_o = 1.2$ ms, compatible with our data range which shows a logarithmic kinetics upon intrusion down to the lowest investigated time of 3 ms. Our data is not compatible with a trial frequency ν_o lower than 500 kHz. Fig. (6) plots the prediction of eq. (14) at $T = 15$°C for 2 trial values of ν_o, 1 MHz and 10 MHz. These two scenarii give two values of $P_{int,o}$which differ only of 3.3 MPa. Therefore the value of $P_{int,o}$ depends weakly on the choice made for the value of ν_o. Assuming that the frequency ν_o actually lies in the range 1-10 MHz, we get a solid surface energy of the strongest hydrophobic defects $(\gamma_{SL}-\gamma_{SV})_s$ in the interval 41.5 to 43.5 mN/m, and a contact angle θ_s between 119° and 123°. These values are slightly higher than the ones found in MCM41 of comparable pore size, with the same silanization procedure (i.e. an internal surface energy $\gamma_{SL}-\gamma_{SV}$ of 36 mN/m and a contact angle of 120°[12]). We attribute this to the slighlty larger grafting density achieved in the PMOs (see section II A).

C. Ageing of the grafted silanes

A slow ageing of the material is observed according to the cumulated time t_{fil} the material spends at high pressure, filled in water. The upper graph in Fig. 7 shows the evolution of P_{int} according to t_{int} for three times t_{fil}. This cumulated time t_{fil} reaches 4.3 h at the end of the whole set of experiments carried out with this sample. The downward shift of P_{int} on the full range of considered t_{fil} is of the order of 10 MPa, that is significantly more than the modest difference in intrusion pressure measured between 5 and 45°C. This ageing can first be characterized by a decrease of the equilibrium pressure P_{eq}. Based on measurement at room temperature, P_{eq}, initially close form 54 MPa, loses around 2 MPa during the first cycles and then follows an almost linear decrease with a slope of -2.3 MPa/h of cumulated filled time t_{fil} (see inset of Fig. 7 and table III). This decrease is nevertheless sufficiently slow to be able to characterize, on short time scale, the material in a quasi-identical state as illustrateded by the superimposition of two independent set of measurements for t_{fil} close from 2.5 h. In particular, it is possible to characterize intrusion pressures for various temperatures for a quasi-identical state of the material as previously discussed. From a fit of Eq 14 on experimental dynamical pressures measured at several t_{fil} values, the decrease of P_{eq} is accompanied by a decrease of $P_{int,o}$ corresponding to a decrease of θ_s (see table III). Considering an intermediate cut-off time $t_o = 0.6$ ms, based on considerations detailed in section IV B, θ_s decrease from 125° at short time to 119° for $t_{fil} = 4.3$ h. This decrease, which is related to the evolution of the surface energy of the regions with stronger hydrophobicity, can be attributed to the hydrolysis of the grafting agent. Beyond the decrease of θ_s, the fitting of experimental points reveal also a decrease of the volume V_s,

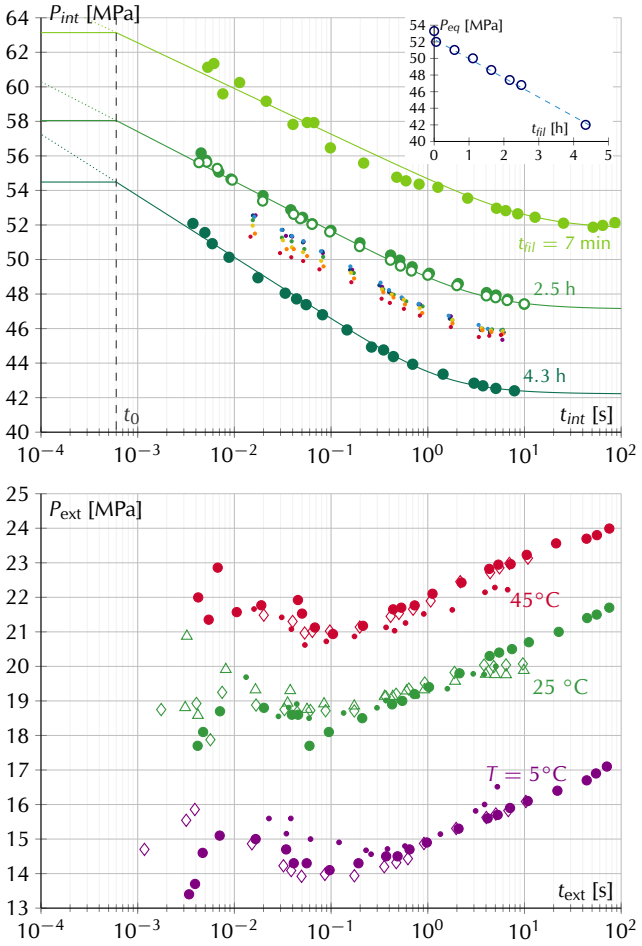

FIG. 7. Upper graph: Intrusion P_{int} according to t_{int} at $T = 25$°C (large green points) for three values of t_{fil} (see text). Intrusion pressures presented in Fig. 3 measured for a similar t_{fil} but various temperatures are recalled for comparison (rainbow series of small dots). Plain curves are fits of Eq. 14. Lower graph: Extrusion P_{ext} according to t_{ext} for $t_{fil} < 1$ h (full circle), $t_{fil} = 2.5$ h (open diamond) and $t_{fil} = 4.5$ h (open triangle) and for three temperatures. Extrusion pressures presented in Fig. 3 for these three temperature are recalled for comparison (small dots).

from 3.6 nm^3 at short t_{fil} down to 2.9 nm^3 for $t_{fil} = 4.3$ h. Such a decrease of V_s corresponds to a reduction of l_s which is also coherent with the suggested hydrolysis process.

TABLE III. Raw parameters obtained from fitting the intrusion pressure Eq (12): V_s, P_{eq} and τ. The equilibrium pressure $P_{int,o}$ and the corresponding contact angle θ_s are calculated using $R_p = 1.3$ nm, and an intermediate cut-off time $t_0 = L_p/(\lambda v_0) = 0.6$ ms.

t_{fil} h	V_s nm^3	P_{eq} MPa	τ s	$P_{int,o}$ MPa	θ_s °
0.12	3.6	51.7	12	63.1	125
2.5	3.3	47.1	3.67	58.0	122
4.3	2.67	42.2	1.66	54.5	119

TABLE IV. Extrusion volume V_{ext}, pore radius $R_{extrusion} = (V_{ext}/4.26)^{1/3}$, and three-phase line tension σ, derived from the extrusion pressure using eq. (20). $P_{ext,min}$ is the minimum observed extrusion pressure.

T °C	V_{ext} nm^3	$R_{extrusion}$ nm	$P_{ext,o}$ MPa	σ pN
5	8.37±1.5	1.25±0.08	19.8	-16±2
10	9.9±0.5	1.32 ± 0.03	19.8	-18.5 ±2
15	8.12 ±0.4	1.24 ± 0.03	20.2	-15± 2
25	11 ±0.8	1.37 ± 0.03	21.6	-20.5±2
30	13 ±1	1.4 ± 0.04	22.5	-22± 2
35	9.38 ±0.5	1.3 ± 0.03	23.2	-18.5 ± 2
45	10.54 ±0.7	1.35 ± 0.03	23.5	-20± 2

Surprisingly, unlike P_{int}, P_{ext} is independent of t_{fil} (see lower graph in Fig 7). The extrusion pressure measured at three different temperatures for several value of t_{fil} remains the same for each temperature whatever t_{fil}. This fact strongly suggest that the phenomenon which controls the dynamical extrusion pressure is different from the one which controls the intrusion pressure. Considering that P_{int} is controlled by a thermally activated wetting, P_{int} depends on the structure and physisco-chemical properties of the whole surface of the pores. A statistical degradation of the grafting is thus revealed by the measurement of P_{int}. If P_{ext} is controlled by a local bubble nucleation process, as further justified in the next section, a single locus in each pore only matters. As long as some hydrophobic spots are preserved in each pores, the extrusion pressure might not be affected by the average chemical ageing of the pores. Nevertheless it is particularly striking that a slow decrease of the average hydrophobicity of the material do not impact at all the extrusion pressure (for extreme t_{fil} values, much larger than the one considered here, it is expected however that the extrusion pressure would eventually decrease when the grafting begins to be fully degrated). Another striking event that is specific to extrusion is the short time cut-off between 10^{-2} s and 10^{-1} s.

V. COMPARISON WITH EXPERIMENTAL RESULTS: EXTRUSION.

Water extrusion from the PMOs exhibits a logarighmic kinetics at times larger than 100 ms. The activation volumes extracted from the slope of this logarithmic characteristics (see figure 3) are listed in table IV.

Two mechanisms require in principle a thermal activation for the extrusion process to occur: the first one, already considered in homogeneous silica-tempated mesopores[12,15], is the nucleation in each pore of a vapor bubble spanning the pore width, resulting in the creation of two independant meniscii. The second is the activated dewetting process studied in section (III), due to the weakly hydrophobic portions of the pore.

Regarding the qualitative differences and dissymmetries between the intrusion and extrusion logarithmic kinetics, it seems unlikely that heterogeneous dewetting is the mechanism limiting extrusion. A first dissymmetry is the temperature dependancy of the extrusion process, much larger than upon intrusion, and reminiscent to the one observed in MCM41[15]. Indeed in the case of heterogeneous (de)wetting, the energy barrier involves only solid surface tensions (see eq. 11) and is thus essentially independant of the temperature. The temperature effect arises only from the Arrhenius factor and affects the slope of the logarithmic kinetics, as is indeed observed for the intrusion pressure. To the contrary the energy barrier for the bubble nucleation involves a liquid/vapor interface and is itself a temperature-dependant quantity. This was shown to contribute to a temperature effect not only on the slope of the pressure/log time characteristics, but also on its offset[15].

A second dissymmetry is the short-time cut-off of the extrusion logarithmic kinetics, which appears as a strong feature disqualifying heterogeneous dewetting as a limiting mechanism. In a periodically alternating system such as the PMOs the activated wetting and dewetting process are intrinsically symmetric from the point of view of the time window, whereas no short-time cut-off is observed at intrusion.

For these reasons we compare the measured activation volume extracted from the logarithmic kinetics at extrusion, to the model of the bubble nucleation. We use here the analytic model derived by Lefevre et al[12] for a homogeneous cylindrical pore, as we are not aware of a theory taking into account heterogeneities. The energy barrier writes:

$$\Delta\Omega = P_{ext} K_1(\theta) R_p^3 + \gamma_{LV} K_2(\theta) R_p^2 + K_3(\theta)\sigma R p \qquad (19)$$

where the K_i's are functions of θ and σ is the 3-phase line tension, from which the extrusion pressure expresses as:

$$P_{ext} = \frac{k_B T}{K_1(\theta) R_p^3} \ln \frac{t_{ext} \nu L}{R_p} - \frac{K_2(\theta)\gamma_{LV}}{K_1(\theta) R_p} - \frac{\sigma}{R_p^2} \frac{K_3(\theta)}{K_1(\theta)} \qquad (20)$$

A value $R_{extrusion}$ of the pore radius is derived from the measured activation volume $V_{ext} = K_1(\theta) R_{extrusion}^3$. For $112^\circ \leq \theta \leq 125^\circ$, $K_1(\theta) = 4.26 \pm 0.02$, therefore the largest uncertainty in the evaluation of $R_{extrusion}$ comes from the experimental error bar on V_{ext}. The values found for $R_{extrusion}$ (see table IV) are very similar to the radius R_s of the strongly hydrophobic part of the pore, which is coherent. This provides a further evidence of a nucleation-limited extrusion.

As a consequence, the extrusion kinetics does not reflect the specific characteristics of the weakly hydrophobic portions of the pores. It is nevertheless possible to compare the measured values of the extrusion pressure to the indirectly evaluated nominal pressure on these weakly hydrophobic defects, according to eq (18): $P_{ext,o} = P_{eq} + k_B T/V_w \ln(\tau/t_o)$. With the same hypothesis than in section IV, i.e. a short cut-off time between 0.12 and 1.2 ms, the lowest found values of P_{ext},o reported in table (IV) are slightly larger than the measured values. Therefore, once nucleated, a vapor bubble should grow and reach the entrances of the pore without need of further activation to overcome the weakest hydrophobic parts of the pores.

Finally we report the values found for the line tension σ, although its physical meaning is only indicative of an order of magnitude as the contact line crosses the chemically different portions of the pore. The negative sign and order of magnitude of 15 to 20 pN is similar to the one found in silane-grafted templated mesoporous silicas[15].

VI. CONCLUSION

In conclusion we show that dynamic experiments of intrusion/extrusion of water in model hydrophobic nanopores provide an unprecedented approach to characterize the internal features of pore pattern, in terms of sizes and surface energies in relation with wetting dynamics at ultimate scale. In addition to a single value of the intrusion and extrusion pressure, the logarithmic variation of the pressure with the process time (or rate) allows to determine activation volumes yielding informations on the internal characteristic sizes, and further information is gained from the time window of the logarithmic kinetics.

In the silane-grafted hybrid PMOs, the logarithmic kinetics of the intrusion process is in very good agreement with a classical model of thermally activated heterogeneous wetting. We derive the size of the silane-grafted periodic portions of the PMOs, the Cassie-Baxter average wettability, as well as the contact angle of water on the grafted portions. These characteristics meet the known structural properties of PMOs, in particular the length of hydrophobic portions, identified from our mechanical characterization is compatible with the periodicity of 0.77 nm reported in PMO. They are also compatible with previous work on silane-grafted mesoporous micelle-templated silicas.

We also show that the extrusion process in the hybrid PMOs is governed by a vapor nucleation mechanism, and not by thermally activated heterogeneous dewetting. Due to the small size of the periodic pattern with respect to the pore radius, the nucleation process is comparable to the one studied previously in homogeneous cylindrical pores, and the critical nucleation volume is found to yield an accurate value of the pore radius.

Finally it is of interest to compare in more details the intrusion/extrusion of water in hybrid PMOs and in homogeneous MCM-41, as these model mesoporous media have a comparable nominal pore size (1.95 nm for the PMOs and 2.07 nm for the MCM41) and are silanized using the same procedure[12,15]. In Guillemot et al[15] no logarithmic dynamics was observed upon intrusion, in the limit of an experimental resolution of 0.2MPa/decade somewhat lower than in the present work. This resolution did not allow to detect an activation lower than 50 nm[3], corresponding to an average distance between potential grafting defects larger than 10 nm. The logarithmic kinetics of intrusion evidenced in the PMOs is indeed a distinctive property of the hybrid material and its wetting heterogeneity. To the contrary the extrusion kinetics is quite similar in the two materials, from the point of view of the activation volumes and temperature dependancy. The only qualitative difference lies in the small time cut-off of the logarithmic kinetics. The latter is found here to be limited to 100 ms in the PMOs, whereas in the MCM-41 a limitation of the logarithmic kinetics was indeed observed at times lower than 10 ms. We have no explanation for this difference and further work is under progress to understand the physics of the extrusion process at high rate.

ACKNOWLEDGMENTS

This work was supported by the French Research Agency (ANR LyStEn 15-CE06-0006). We are strongly grateful to Anne Galarneau who suggested initially the usage of PMOs. We thank Jérome Giraud for experimental developments and Charles Josserond for the implementation of our experiments on traction machines at SIMAP laboratory.

DATA AVAILABILITY STATEMENT

The data that support the findings of this study are available from the corresponding author upon reasonable request.

Appendix A: PMOs synthesis and grafting

Mesoporous benzene-silica PMO is synthesized following the protocol proposed by Inagaki *et al*[27]. A solution of 20 g of sodium hydroxide (NaOH) at 6M, 8.35 g of octadecyltrimethylammonium (ODTMA) and 10 g of 1,4-Bis(triethoxysilyl)benzene (BTEB) is prepared in 250 mL of distilled water and left for 21 h at room temperature under strong agitation to dissolve BTEB and homogenize its concentration. The solution, at rest, is then heated at 95°C for 20 h leading to the formation of a white precipitate (4.1 g) which is collected and thoroughly rinsed with pure water. Reflux extraction of the surfactant (ODTMA) is carried out at 70°C for 8 h with a solution of 250 mL of 95% ethanol, and 7.6 mL of 37% hydrochloric acid for 1 g of PMO powder. After surfactant extraction, the powder is dried at 40°C for 24 h and stored in vial.

To reach a high level of hydrophobicity, the silica regions of the so obtained PMO are functionnalized following Lefevre et al[12]. The grafting procedure starts degassing 500 mg of PMO at 0.1 mbar and 150°C for 20 h. The powder is then supplemented with 20 mL of anhydrous toluene, 1 mL of

anhydrous pyridine and 2 mL of octyldimethylchlorosilane (grafting agent) under argon atmosphere. The grafting last 7 h at 120° with a slight agitation. The powder is then filtrated and thoroughly washed successively with toluene, acetone and ethanol. The powder is finally dried 2 h at 80°C and then 5 h at 0.1 mbar and 100°C in a partially open vial.

Appendix B: Pore size characterization

The powder X-ray diffraction pattern of the so-obtained native material (see Fig. 8 is characteristic of a two-dimensional hexagonal lattice, the first peak of the spectrum correspond to an inter-reticular distance of 4.6 nm.

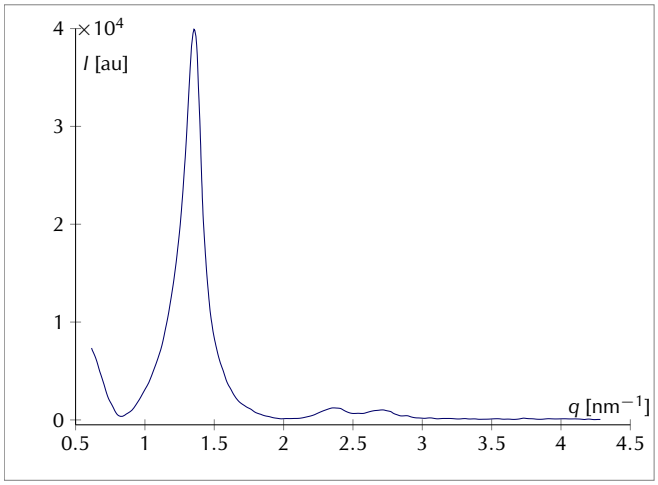

FIG. 8. X-ray diffractogram of the native PMO sample after substraction of the base line. The main pic at $q = 1.35$ nm^{-1} corresponds to an inter-reticular distance of 4.65 nm.

The inner pore radius is deduced from nitrogen adsorption isotherms presented in Fig. 9. The model used to fit experimental points is based on the dependence of the thickness t of a prewetting film according to the chemical potential imposed by the vapor pressure p, taking into account capillary effects and disjoining effects in cylindrical pores. Filling of a pore by capillary condensation occurs when the grand potential of the pre-wetting film becomes larger than the grand potential of the completely filled pores[28]. In the prewetting regime the disjoining pressure is classical modeled as $\Pi = H_{slv}/(6\pi t^3)$ where H_{slv} is the Hamaker constant corresponding to the non retarded van der Waals interactions between the solid and the vapor through the liquid film. This model is valid only beyond a threshold thickness[28] $t_s = \sqrt{H_{slv}/(4\pi S)}$. An estimate of this thickness with $H_{slv} \sim 10^{-19}$ J/m^2 leads to a value of $0.34R_p$ in the grafted material of average radius R_p which is close to the typical thickness measured at capillary condensation, and thus prevent the usage of the previous expression for Π in the prewetting regime. More generally, for small mesopores, as considered here, it turns out that the disjoining pressure should rather be modeled as an exponential decay[29,30]. The inset of Fig. 9 shows, for the native PMO of raidus R_w, the logarithm of the dimensionless disjoining pressure Π in the prewetting region ($\ln(p/p_0) < -1.5$ with p_0 the saturation pressure) which is perfectly linear according to t/R_w. Such a behavior is precisely in agreement with a model of the form $\Pi = S/\xi \exp(-t/\xi)$ where S is the spreading parameter and ξ an interaction length[29,30]. On the contrary, trying to fit the classical $\propto t^{-3}$ model leads to the dashed line which confirms its inadequacy. Fitting of the prewetting region allows the identification of S and ξ and an average pore radius. We find $S = 0.07$ J/m^{-2}, $\xi = 0.24$ nm and $R_w = 1.95$ nm for the native material. It is worth mentioning that the so obtained S and ξ value are almost identical to the one obtained with a MCM-41 with a radius of 2.4 nm[30]. For the grafted material we get $S = 0.03$ J/m^2, $\xi = 0.25$ nm and $R_p = 1.5$ nm. The identified values of R_w and R_p imposes also the position of the capillary condensation (dashed curves in Fig. 9). This position agrees with the presumable condensation in both type of pores, nevertheless as the condensation is not sharp especially in the grafted material, the limit between the prewetting regime and the beginning of the condensation is not obvious. To be able to incorporate in the fitting procedure the points corresponding to the capillary condensation region, we consider a gaussian distribution of the pore size (which artificially helps to take also into account the presence of periodic defects). This leads to the identification of the standard deviation σ of this distribution as an additional parameter. For the native material (plain red line in Fig. 9) we find $\sigma/R_w = 0.15$ while for the grafted material (plain blue curve) we find a larger value $\sigma/R_p = 0.2$ attributed to the periodic grafting.

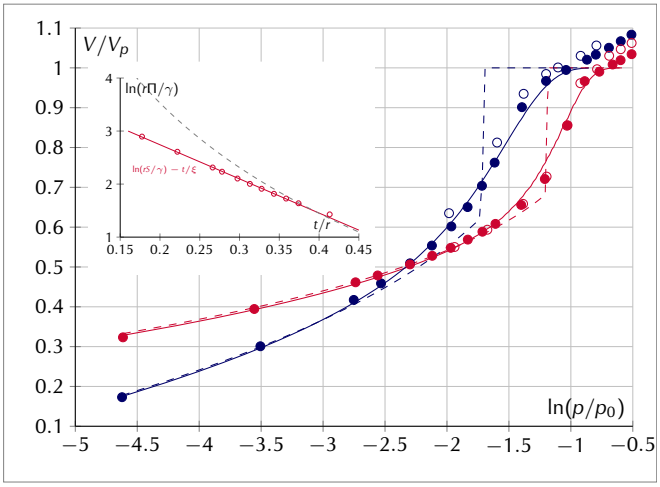

FIG. 9. Adsorption (full symbols) and desorption (open symbol) isotherms of nitrogen at 77 K in native material (red points) and in silanized material (blue points) with V_p the total pore volume measured just after condensation. Lines are fits of a model of a prewetting film up to capillary condensation (see text) for a single pore size (dashed line) or gaussian pore size distribution (plain line). Inset: logarithm of the dimensionless disjoining pressure Π according to the dimensionless film thickness in the low pressure range for the native material. Dots are experimental points. The full line is a linear fit corresponding to $\Pi = S/\xi exp(-t/\xi)$ with S the spreading parameter and ξ an interaction length. Dashed line is the best fit considering $\Pi \propto t^{-3}$.

[1] G. Fraux, F.-X. Coudert, A. Boutin, and A. Fuchs, Chem. Soc. Rev. **46**, 7421 (2017).
[2] V. Eroshenko and A. Fadeev, Colloid Journal **57**, 446 (1995).
[3] A. Fadeev and V. A. Eroshenko, J. Coll. Interf. Sci. **187**, 275 (1997).
[4] V. A. Eroshenko, R. C. Regis, M. Soulard, and J. Patarin, J. Am. Chem. Soc. **123**, 8129 (2001).
[5] A. Han and Y. Qiao, J. Mat. Res. **22**, 644 (2007).
[6] G. Ortiz, H. Nouali, C. Marichal, G. Chaplais, and J. Patarin, J. Phys.Chem. C **118**, 7321 (2014).
[7] I. Khay, T. J. Daou, H. Nouali, A. Ryzhikov, S. Rigolet, , and J. Patarin, J. Phys.Chem. C **118**, 3935 (2014).
[8] J. Canivet, A. Fateeva, Y. Guo, B. Coasne, and D. Farrusseng, Chem. Soc. rev. **43**, 5594 (2014).
[9] M. Michelin-Jamois, C. Picard, G. Vigier, , and E. Charlaix, Phys. Rev. Lett. **115**, 036101 (2015).
[10] J. Beck, J. Vartuli, W. Roth, M. Leonowicz, C. Kresge, K. Schmitt, C. Chu, D. Olson, E. Sheppard, S. McCullen, et al., J. Am. Chem. Soc. **114**, 10834 (1992).
[11] D. Zhao, Q. Hui, J. Feng, B. Chmelka, and G. Stucky, J. Am. Chem. Soc. **120**, 6024 (1998).
[12] B. Lefevre, A. Saugey, J.-L. Barrat, L. Bocquet, E. Charlaix, P. Gobin, and G. Vigier, Journal of Chemical Physics **120**, 4927 (2004).
[13] B. Lefevre, A. Saugey, J.-L. Barrat, L. Bocquet, E. Charlaix, P. Gobin, and G. G. Vigier, Coll. and Surf. A **241**, 265 (2004).
[14] S. Sharma and P. Debenedetti, PNAS **109**, 4365 (2012).
[15] L. Guillemot, T. Biben, A. Galarneau, G. Vigier, and E. Charlaix, PNAS **109**, 19557 (2012).
[16] Y. Grosu, O. Ievtushenko, V. Eroshenko, J. Nedelec, and J.-P. E. JGrolier, Coll. and Surf. A **441**, 549 (2013).
[17] A. Tinti, A. Giacomello, and C. Casciola, Eur. Phys. J. E **41**, 11658 (2018).
[18] M. Amabili, Y. Grosu, A. Giacomello, S. Meloni, A. Zaki, F. Bonilla, A. Faik, and C. Casciola, ACS Nano **13**, 1728 (2019).
[19] P. Van Der Voort, D. Equivel, E. De Canck, F. Goethals, I. Van Driesshe, and F. J. Romero-Salguero, Chem. Soc. Rev. **42**, 3913 (2013).
[20] A. Ryzhikova, T. J. Daoua, H. Noualia, J. Patarin, J. Ouwehand, S. Clerick, E. De Canck, P. Van Der Voort, and J. Martens, Microporous and Mesoporous Materials **260**, 166 (2018).
[21] T. Blake, J. Colloid Interface Sci. **299**, 1 (2006).
[22] E. Rolley and C. Guthman, Phys. Rev. Letter **98**, 166105 (2007).
[23] K. Davitt, M. Pettersen, and E. Rolley, Langmuir **29**, 6884 (2013).
[24] D. Guan, E. Charlaix, and P. Tong, Phys Rev Lett **124**, 188003 (2020).
[25] N. Mizoshita, T. Tani, and S. Inagaki, Chemical Society reviews **40**, 789 (2011), ISSN 0306-0012.
[26] J. G. Croissant, X. Cattoën, M. Wong Chi Man, J.-O. Durand, and N. M. Khashab, Nanoscale **7**, 20318 (2015), URL `http://dx.doi.org/10.1039/C5NR05649G`.
[27] S. Inagaki, S. Guan, T. Ohsuna, and O. Terasaki, Nature **416**, 45 (2002).
[28] J.-M. di Meglio, D. Quere, and F. Brochard-Wyart, Compte-Rendus de l'Académie des Sciences **309**, 19 (1989).
[29] R. J. Pellenq, B. Coasne, R. O. Denoyel, and O. Coussy, Langmuir **25**, 1393 (2009), ISSN 07437463.
[30] I. Deroche, T. J. Daou, C. Picard, and B. Coasne, Nature Communications **10**, 1 (2019), ISSN 2041-1723, URL `http://dx.doi.org/10.1038/s41467-019-12418-9`.
[31] A. Ryzhikov, T. J. Daou, H. Nouali, J. Patarin, J. Ouwehand, S. Clerick, E. D. Canck, P. Van Der Voort, and J. A. Martens, Microporous and Mesoporous Materials **260**, 166 (2018), ISSN 1387-1811, URL `https://doi.org/10.1016/j.micromeso.2017.10.037`.
[32] H. Gayvallet and E. Charlaix, J. Phys. II France **2**, 2025 (1992).
[33] V. Gérard, Ph.D. thesis, UGA Grenoble (2010).
[34] M. Bossert, A. Grosman, I. Trimaille, C. Noûs, and E. Rolley, Langmuir **36**, 11054 (2020).
[35] E. Rolley, N. Garroun, and A. Grosman, Phys. Rev. B **95**, 064106 (2017).
[36] S. Marchio, S. Meloni, A. Giacomello, and C. Casciola, Nanoscale **11**, 21458 (2019).
[37] P. Giovambattista, N.and Rossky and P. Debenedetti, Phys. Rev. Lett. **102**, 050603 (2009).
[38] G. Giovambattista, P. Debenedetti, and P. Rossky, J. Phys. Chem. C **111**, 1323 (2007).
[39] L. Guillemot, A. Galarneau, G. Vigier, T. Abensur, and E. Charlaix, Rev. of Scientific Inst. **83**, 105105 (2012).
[40] L. Tzanis, M. Trzpit, M. Soulard, and J. Patarin, J. Phys.Chem. C **116**, 20389 (2012).
[41] C. T. Kresge, M. E. Leonowicz, W. J. Roth, J. C. Vartuli, and J. S. Beck, Nature **359**, 710 (1992).
[42] P. Aryal, M. Sansom, 3, and S. Tucker, J. Mol. Biol. **427**, 121 (2015).
[43] A. Grosman and C. Ortega, Phys. Rev. B **78**, 085433 (2008).
[44] A. Fadeev and V. A. Eroshenko, J. Coll. Interf. Sci. **187**, 275 (1997).
[45] A. Fadeev and V. Eroshenko, Colloid J. **58**, 654 (1996).